


## Research Article

# Application of Adaptive PID Temperature Control Algorithm under Spatial Thermal Model of ALD Reaction Chamber

Zhenqiang Liu,<sup>1</sup> Jinhui Lei<sup>1</sup> ,<sup>1</sup> Yan Chen,<sup>1</sup> Yang Xia,<sup>2</sup> Jiaheng Feng,<sup>2</sup> Shuaiqiang Ming,<sup>2</sup> and Wa Mao<sup>1</sup>

<sup>1</sup>*School of Information Engineering and Automation, Kunming University of Science and Technology, Kunming, Yunnan 650500, China*

<sup>2</sup>*Kemin Electronic Equipment Technology co., LTD, Jiaxing, Zhejiang 314000, China*

Correspondence should be addressed to Jinhui Lei; [ljh13700650851@163.com](mailto:ljh13700650851@163.com)

Received 10 February 2022; Revised 28 February 2022; Accepted 16 March 2022; Published 11 April 2022

Academic Editor: Wen Zeng

Copyright © 2022 Zhenqiang Liu et al. This is an open access article distributed under the Creative Commons Attribution License, which permits unrestricted use, distribution, and reproduction in any medium, provided the original work is properly cited.

The study aims to expand the application of the proportion integral derivative (PID) algorithm and improve the practical application of the PID algorithm to the atomic layer deposition (ALD) process. First, the ALD process is analyzed, and the application method of the PID algorithm is determined. Second, the research conditions of the PID algorithm based on the ALD process are designed. Finally, the temperature control operation of the PID algorithm in the ALD reaction chamber is modeled and experimentally studied under different research conditions. The results show that temperature significantly impacts the reaction chambers of stainless steel and aluminum. When the heating temperature increases, the temperature of the stainless steel chamber will also change, and the maximum difference between the chamber and the heating temperature is about 33°C. In contrast, the temperature of the aluminum chamber varies little with the heating temperature. The maximum difference between the chamber temperature and heating temperature is about 350°C, which shows that the temperature of the stainless steel chamber is better controlled and is more practical under the same temperature conditions. The pressure change has little effect on the temperature change of the reaction chamber of the two materials. The temperature curves of the two chambers show that the PID temperature control system can be used normally and has strong practicability. The study provides technical support for improving the PID temperature control system and the rational use of the PID temperature control algorithm in the ALD process.

## 1. Introduction

In recent years, atomic layer deposition (ALD) technology has attracted extensive attention because of its accurate material synthesis and modification characteristics (precise to nuclear scale). In particular, ALD is excellent in researching and developing new nanocatalytic materials [1]. Moreover, the PID (proportional, integral, and differential) temperature control algorithm to the ALD process can effectively control the temperature of the ALD reaction chamber, provide a suitable reaction environment for the ALD process, and improve the production speed [2]. Although the application of the PID temperature control algorithm to

the ALD process is not perfect, many studies provide technical support for the application of the PID temperature control algorithm.

Gilbert and Leeuwen (2020) pointed out that ALD is a thin film growth technology with surface self-limiting reaction, and it can accurately control the growth of thin films. There is no ALD alumina reaction group on the surface of polyolefin membrane, resulting in the slow growth and nucleation of ALD alumina and the low reaction efficiency in the early stage. The final development of alumina primarily forms clusters rather than intact and covered films [3]. Tomer et al. (2019) argued that temperature uniformity in the reaction chamber could be well solved by using the

partition heating method, the PID controller with anti-integral saturation method, and the feed forward compensation PID control algorithm [4]. Huang et al. (2018) pointed out that temperature control is a concern of most industrial enterprises. The temperature control quality directly affects the quality of products and the efficiency of enterprises. However, temperature control accuracy is low due to temperature-controlled components' different characteristics, and the adjustment time is long in actual production [5]. Li et al. (2020) pointed out that the PID algorithm can automatically identify different parameters according to the actual situation, which significantly simplifies the debugging process and saves time. The response and accuracy of temperature control are improved, which has a tremendous practical effect on enhancing efficiency [6].

Grillo et al. (2018) argued that the temperature control system is designed, including hardware and software design. Finally, the response ability and stability of the steep curve of the PID algorithm are tested by a simulation experiment. The results show that the system has a fast response ability and strong strength, which improves temperature control accuracy [7]. Mu et al. (2019) uttered that ALD is a nanofilm preparation technology. The controllable thickness and uniform film could be obtained by self-restrictive precursor alternating saturation reaction. It could be used as a water-insulating and oxygen-insulating layer in electronic devices, a transistor gate dielectric layer, and a surface passivation layer of solar cells. Therefore, ALD is widely used in microelectronics, solar cells, flexible electronics, and other fields. Temperature is one of the most critical factors affecting the quality and efficiency of thin films. However, the existing conventional control methods have poor temperature stability, long stability adjustment time, and significant temperature fluctuation under the condition of external interference, which directly affects the microsurface morphology of the deposited thin film. The PID temperature control algorithm can improve the transient performance of the system through rolling optimization and output correction under external interference. It has the characteristics of processing time delay, constraint ability, and low requirement for mathematical model. It has been successfully applied in the field of automatic control and temperature control [8].

In summary, applying the PID temperature control algorithm to the ALD process is not perfect. ALD and the PID temperature control algorithm are introduced and analyzed in this case. Then, the research method of PID temperature control algorithm under different temperature and pressure conditions is designed according to the characteristics of ALD and PID. On this basis, the research model is implemented. Finally, the PID temperature control algorithm in the ALD reaction chamber is comprehensively analyzed through experiments. This research provides new ideas for using the PID temperature control algorithm to control the temperature in the ALD reaction chamber. The utilization rate of the PID temperature control algorithm in the ALD production process is improved, and the production quality and efficiency of ALD are enhanced.

## 2. Research Methods

*2.1. Methodology and Theory.* ALD is used to manufacture nanodevices, and it is a chemical vapor deposition technology [9]. It is a film growth technology with a surface self-limiting reaction, which can accurately control the growth of films. ALD coats the polyolefin membrane to produce a composite membrane of nanoalumina polyolefin. There is no ALD alumina reaction group on the surface of the polyolefin membrane, which results in slow growth and nucleation of ALD alumina and low reaction efficiency, making most of the final grown alumina forms clusters rather than completely covered films. The system of ALD is very complex. The whole system mainly includes a gas pipeline, precursor container, control system, reaction chamber, and vacuum pump. The reaction chamber comprises a wafer, vacuum chamber, and surrounding resistance wire [10]. The internal temperature control of the ALD vacuum reaction chamber is nonlinear, hysteretic, and time-varying. The materials inside the vacuum chamber should be stainless steel, aluminum, quartz, and graphite, which can meet all the above requirements [11]. The basic working process of ALD is that the bottom of the chamber is connected with the vacuum pump to pump air inside the chamber. Then, the precursor enters the vacuum chamber through the electromagnetic switch. Finally, the liquid in the precursor enters the reaction chamber through the gas pipeline to complete the reaction [12]. The reaction process of ALD is shown in Figure 1.

Figure 1 shows that the ALD reaction system includes a gas pipeline, a precursor container, a control system, a reaction chamber, and a vacuum pump. The combination of the control system and the vacuum pump provides power for the whole system. The reaction completes if the liquid in the precursor gasifies and enters the vacuum reaction chamber [13]. After each ALD reaction, the chemicals generated are rinsed with N<sub>2</sub> to remove the determinations, and finally, a complete deposited film is formed [14]. Figure 2 shows the circulation flow of ALD.

Figure 2 shows that the flow of the ALD process is controlled by programmers ( $t_1$ ,  $\Delta t_1$ ,  $t_2$ ,  $\Delta t_2$ ,  $t_3$ ,  $\Delta t_3$ ) to generate 2D materials. A digital control system carries out the ALD process. In the production process of the ALD process, if you need to improve the quality and efficiency of process production, you can improve the cycle times of the ALD process and keep the temperature appropriate in the cycle process. Figure 3 shows the basic software configuration in the ALD control system.

Figure 3 shows that each link of the ALD process can be managed separately in the control software. The PID adaptive temperature control system in the ALD reaction chamber can control the temperature of ALD in real time and ensure that the liquid in the precursor can be gasified normally and enter the reaction chamber smoothly, promoting the complete reaction in the reaction chamber [15]. And the temperature in the ALD reaction chamber can keep high through PID temperature control technology to increase the number of ALD cycles and improve production efficiency. The PID temperature control algorithm calculates and

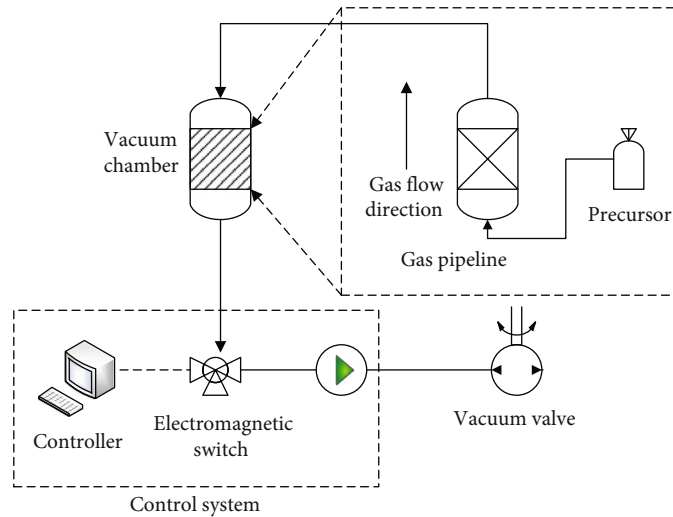


FIGURE 1: ALD reaction system.

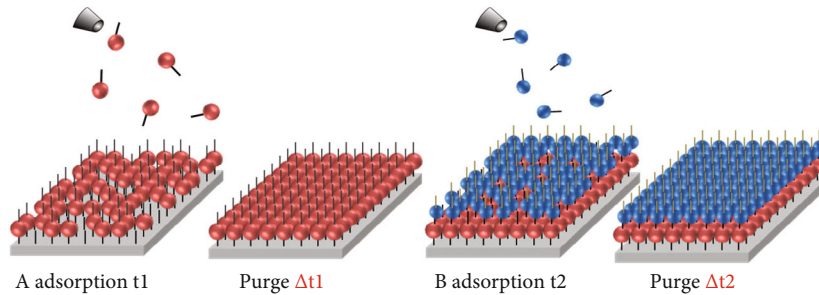


FIGURE 2: Flow of the ALD process.

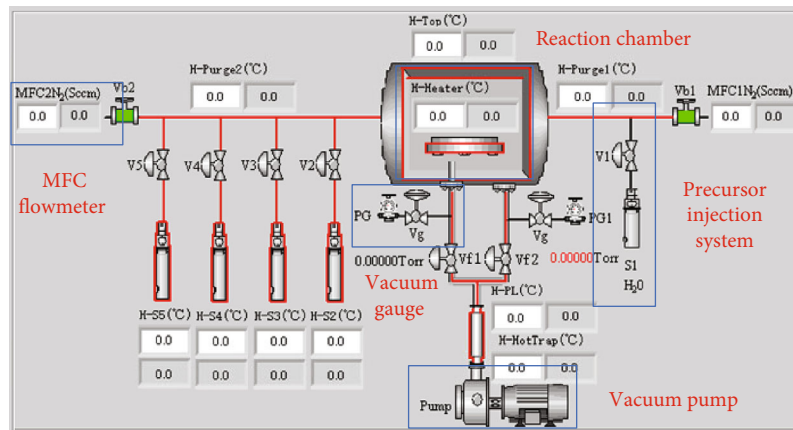


FIGURE 3: Basic configuration of the software in the ALD control system.

controls the system temperature through *P* (proportion), *I* (integral), and *D* (differential) parameters. The PID temperature control system can only predict and adjust the system temperature by adjusting *P*, *I*, and *D* parameters in real time [16]. Figure 4 shows the basic principle of the PID temperature control system.

Figure 4 shows that when the predetermined temperature is set, the PID temperature control algorithm will adjust

the temperature through *P*, *I*, and *D*, making the temperature of the controlled element reach the predetermined value. Real-time feedback will output through the feedback system [17].

2.2. Temperature Control System and ALD Control System. The improved ALD control system can realize the substantial increase of the total output and the

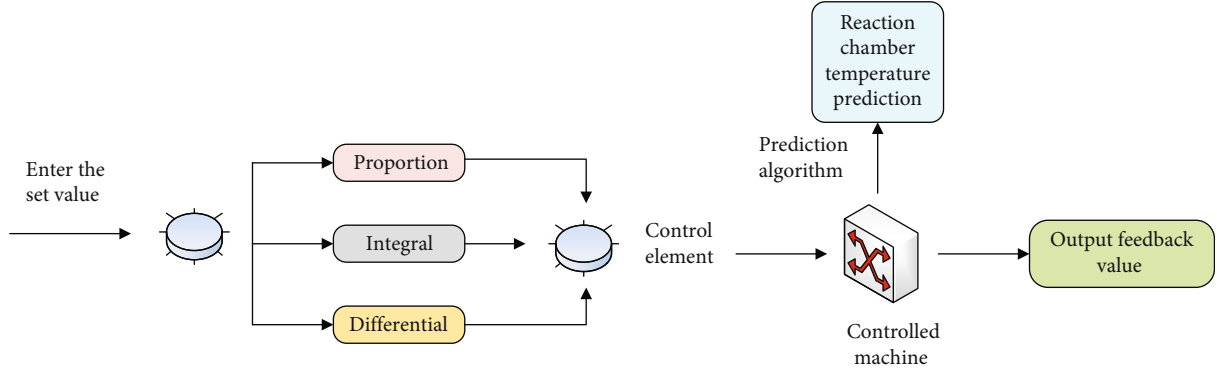


FIGURE 4: Basic principle of the PID temperature control algorithm.

intellectualization of the control system [18]. Usually, an ALD control system consists of an upper computer human-computer interaction system and a lower computer, a vacuum chamber, a temperature control system, and other modules. The upper computer can obtain and interact with data through human operation. When the data are input, the basic parameters of each overall control point are also included [19]. The model of the upper computer is the InTouch configuration software of WonderWare Company. The essential control of the lower computer is realized through the InTouch configuration software. Table 1 shows the basic parameters of the upper computer.

Table 1 shows an advanced host computer operating system, which requires comprehensive upgrading of CPU, a memory card, a hard disk, a graphics card, a system, a program, and a server to obtain more accurate data. In the ALD process, the parameters of all control components are set through the upper computer calculated. The airflow in the vacuum pump is calculated as [20]

$$L_{HFC} = \frac{(KV\rho_{x_2})}{T}, \quad (1)$$

where  $V$  represents the electrical frequency signal,  $\rho_{x_2}$  represents vacuum density,  $T$  represents time,  $L_{HFC}$  represents the gas flow, and  $K$  represents the vacuum parameter in the ALD process reaction chamber. The dynamic pressure inside the vacuum chamber is calculated as

$$\begin{aligned} PV &= \frac{m}{M}RT, \\ P_0 - P &= \frac{RT}{VM} \int_0^t (L_{MFC} - L_{pump}) dt, \\ P &= P_0 - \frac{RT}{VM} \int_0^t (\Delta L) dt, \end{aligned} \quad (2)$$

where  $t$  is the time,  $V$  is the volume inside the chamber,  $P$  is the air pressure inside the chamber,  $M$  is the molar mass of

the gas,  $R$  is the molar constant of the gas,  $T$  is the temperature in the reaction chamber, and  $\Delta L$  represents the gas flow difference in the reaction chamber [21]. The calculation equation of temperature control voltage is

$$U_d = \left(\frac{t}{T}\right)^* U_{AN}, \quad (3)$$

where  $t$  is the time,  $T$  is the cycle time of the voltage pulse, and  $U_{AN}$  represents the average voltage of the pulse. For the temperature test inside the reaction chamber, the temperature of the reaction chamber wafer needs to be measured, and the calculation method adopts the least square method [22]. The calculation equations are as follows:

$$\|\delta\|_2^2 = \sum_{i=0}^m \omega(X_i) [S(X_i) - f(X_i)]^2, \quad (4)$$

$$f(x) = \{(x_i), (y_i), i = 0, 1, \dots, m\}, \quad (5)$$

$$\delta_i = S\left(x_i\right) - y_i, \quad (6)$$

$$\delta_i = S(x_i) - y_i, S(x) = a_0\varphi_0(x) + a_1\varphi_1(x) + \dots + a_n\varphi_n(x), \quad (7)$$

where  $f(x)$  represents the data set and  $S(x)$  represents the fitting curve.  $x_i$  and  $y_i$  represent the dataset of two sets of data, respectively. If the linear independent group of the space where  $s(x)$  is located is  $\varphi_0(x), \varphi_1(x), \dots, \varphi_n(x)$ , the calculation equation of the least square method is

$$\|\delta\|_2^2 = I(a_0, a_1, \dots, a_n) = \sum_{i=0}^m \omega(x_i) \left[ \sum_{j=0}^n a_j \varphi_j(x_i) - f(x_i) \right]^2, \quad (8)$$

$$\frac{\partial I}{\partial a_k} = 2 \sum_{i=0}^m \omega(x_i) \left[ \sum_{j=0}^n a_j \varphi_j(x_i) - f(x_i) \right] \varphi_k(x_i) = 0. \quad (9)$$

TABLE 1: Basic parameters of the upper computer.

Components	Parameters
CPU	Morethanthe3G
Main memory	Morethanthe2G
Hard disk	Morethanthe100G
Graphics card	2GDiscretegraphicscard
System	WindowsXPSP3
Program	Intouch9.6
Server	OPCLink8.0

Equation (9) is used to calculate the minimum value, which is recorded as

$$(\varphi_j, \varphi_k) = \sum_{i=0}^m \omega(X_i) \varphi_j(X_i) \varphi_k(X_i), \quad (10)$$

$$(f, \varphi_k) = \sum_{i=0}^m \omega(X_i) f(X_i) \varphi_k(X_i) = d_k, \quad (11)$$

$$G = \sum_{j=0}^n (\varphi_k, \varphi_j), \quad (12)$$

where  $G\vec{a} = \vec{d}$ . If orthogonal polynomials are used for least-squares fitting,  $G$  is a nonsingular matrix and satisfies the following equations:

$$(\varphi_j, \varphi_k) = \sum_{i=0}^m \omega(x_i) \varphi_j(x_i) \varphi_k(x_i) = \begin{cases} 0, & j \neq k \\ A_k > 0, & j = k \end{cases}, \quad (13)$$

$$a_k^* = \frac{(f, \varphi_k)}{(\varphi_k, \varphi_k)}, \quad (14)$$

where  $a_k^*$  represents the final calculation result. The PID temperature control algorithm controls the temperature of the ALD reaction chamber by changing the initial temperatures, the pressure, and the time gradients. And it is comprehensively studied by comparison [23]. Table 2 shows the conditions for temperature measurement of the ALD reaction chamber.

Table 2 shows that the temperature of the ALD reaction chamber is measured under different initial chamber temperatures and different channels. The time change is as follows: change the initial temperature, last for one hour and record the information; change the initial pressure, last for 15 min; and record the relevant information. And the commonly used stainless steel and aluminum reaction chambers are analyzed in six channels of the ALD reaction chamber. The two reaction chamber materials are compared to determine what materials fit the PID temperature control system. The PID temperature control system is adjusted to make it suitable for more materials and promote its application

TABLE 2: Temperature measurement conditions of the ALD reaction chamber.

Number	Heater	Pumpline	Purge1	Purge2	Hottrap
1	50	150	100	100	400
2	70	150	100	100	400
3	100	150	100	100	400
4	150	150	100	100	400
5	200	150	100	100	400
6	250	150	100	100	400
7	300	150	100	100	400
8	350	150	100	100	400
9	400	150	100	100	400
10	450	150	100	100	400
11	500	150	100	100	400
12	550	150	100	100	400

and development. The comparison between PID and other temperature control algorithms is shown in Table 3.

Table 3 shows that the PID temperature control algorithm is more suitable because of its flexibility, convenient debugging, and high control accuracy.

**2.3. PID Temperature Control Algorithm.** The PID control algorithm comprises a PID regulator, an actuator, and a controlled object [24]. The general calculation equation is as follows:

$$v(t) = Kp \left[ e(t) + \frac{1}{T_j} \int e(t) dt + T_D \frac{de(t)}{dt} \right], \quad (15)$$

where  $v(t)$  represents the output value of the controller,  $e(t)$  represents the error of the control system,  $Kp$  represents the proportional coefficient,  $T_j$  is the integral constant, and  $T_D$  is a constant. When the PID control algorithm is operated by a computer [25], the calculation equation is as follows:

$$v(kT) = K_p \left\{ e(kT) + \frac{T}{T_j} \sum_{i=0}^k e(iT) + \frac{Td}{T} [e(kT) - e(kT - T)] \right\}, \quad (16)$$

where  $v(kT)$  represents the output value when the system is controlled by a computer, and other parameters have the same meaning in Equation (15). The results can also be calculated by an integral coefficient and differential coefficient [26]. The calculation equations are as follows:

$$K_I = \frac{K_p T}{T_I}, \quad (17)$$

$$K_D = \frac{K_p T_D}{T}, \quad (18)$$

$$u(k) = K_p e(k) + K_j \sum_{j=0}^k e(j) + K_D [e(k) - e(k-1)]. \quad (19)$$

TABLE 3: Advantages of the PID temperature control algorithm.

Temperature control algorithm	Advantages	Shortcomings
PID	Easy to debug, high control precision, strong anti-interference ability, high stability ability	Coordination is not good enough
Fuzzy control	Strong robustness and fast response	The parameters are complex and expensive
Neural network control	The algorithm is simple and easy to implement in hardware and software	The system is complex and requires more human coordination

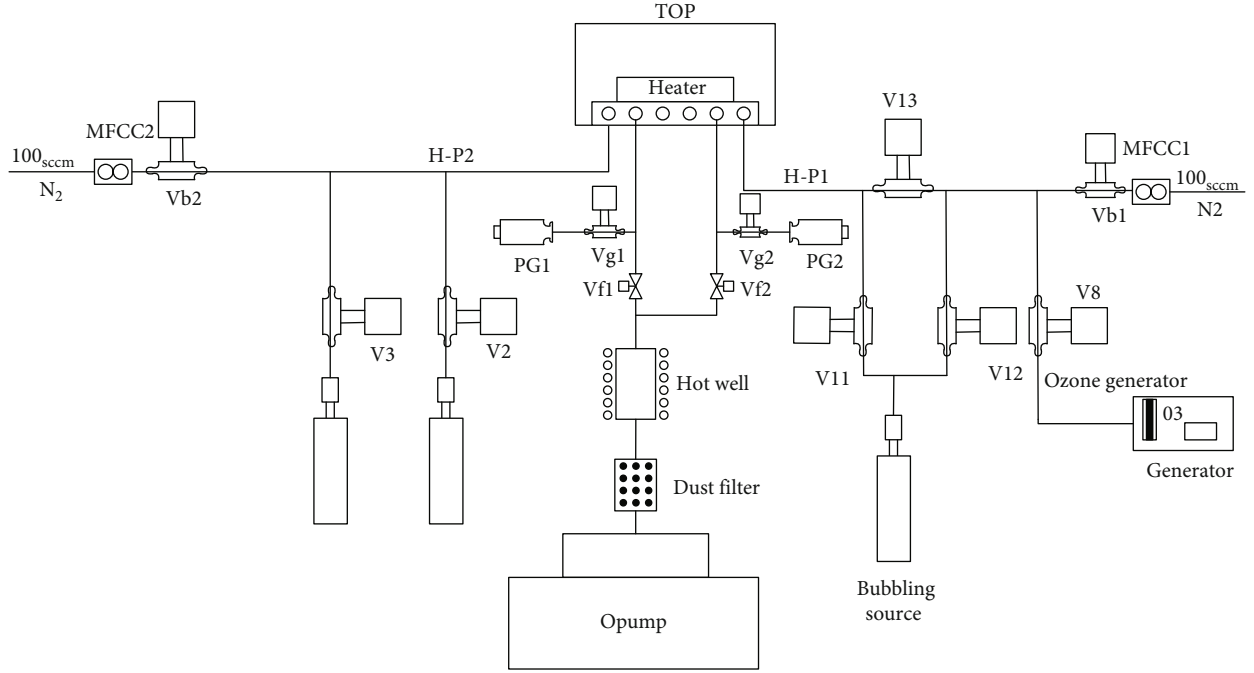


FIGURE 5: Basic framework of the dual-cavity ALD system.

In Equations (17), (18) and (19), (16), and (17) are the calculation equations of integral coefficient and differential coefficient, respectively. And the three equations are used for calculating discrete positions. After a simple calculation is performed, the following equation is obtained [27]:

$$u(k-1) = K_p \left\{ e(k-1) + \frac{T}{T_i} \sum_{j=0}^{k-1} e(j) + \frac{T_D}{T} [e(k-1) - e(k-2)] \right\}, \quad (20)$$

where  $(k-1)$  is the same as the parameter in the above equation, and it is the sampling times in the test process. The following equation is obtained by sorting out Equations (19) and (20) [28]:

$$u(k) - u(k-1) = K_p \left\{ e(k) - e(k-1) + \frac{T}{T_i} e(k) + \frac{T_D}{T} [e(k) - 2e(k-1) + e(k-2)] \right\}. \quad (21)$$

The final calculation equation can be obtained, and it is as follows:

$$u(k) = u(k-1) + K_p \left\{ [e(k) - e(k-1)] + \frac{T}{T_i} e(k) + \frac{T_D}{T} [e(k) - 2e(k-1) + e(k-2)] \right\}. \quad (22)$$

After Equation (22) is simplified, this can be obtained as

$$u(k) = u(k-1) + a_0 e(k) - a_1 e(k-1) + a_2 e(k-2). \quad (23)$$

The position calculation equation of PID in the computer control system is obtained, and the final result needs to be fuzzified. If the input value is defined between  $[-x, x]$  and the fuzzy value is a value in  $\{-m, -m+1, \dots, 0, \dots, m-1, m\}$ , the quantization factor of the fuzzy value can be calculated [29]. The calculation equation is

$$t = \frac{m}{x}, \quad (24)$$



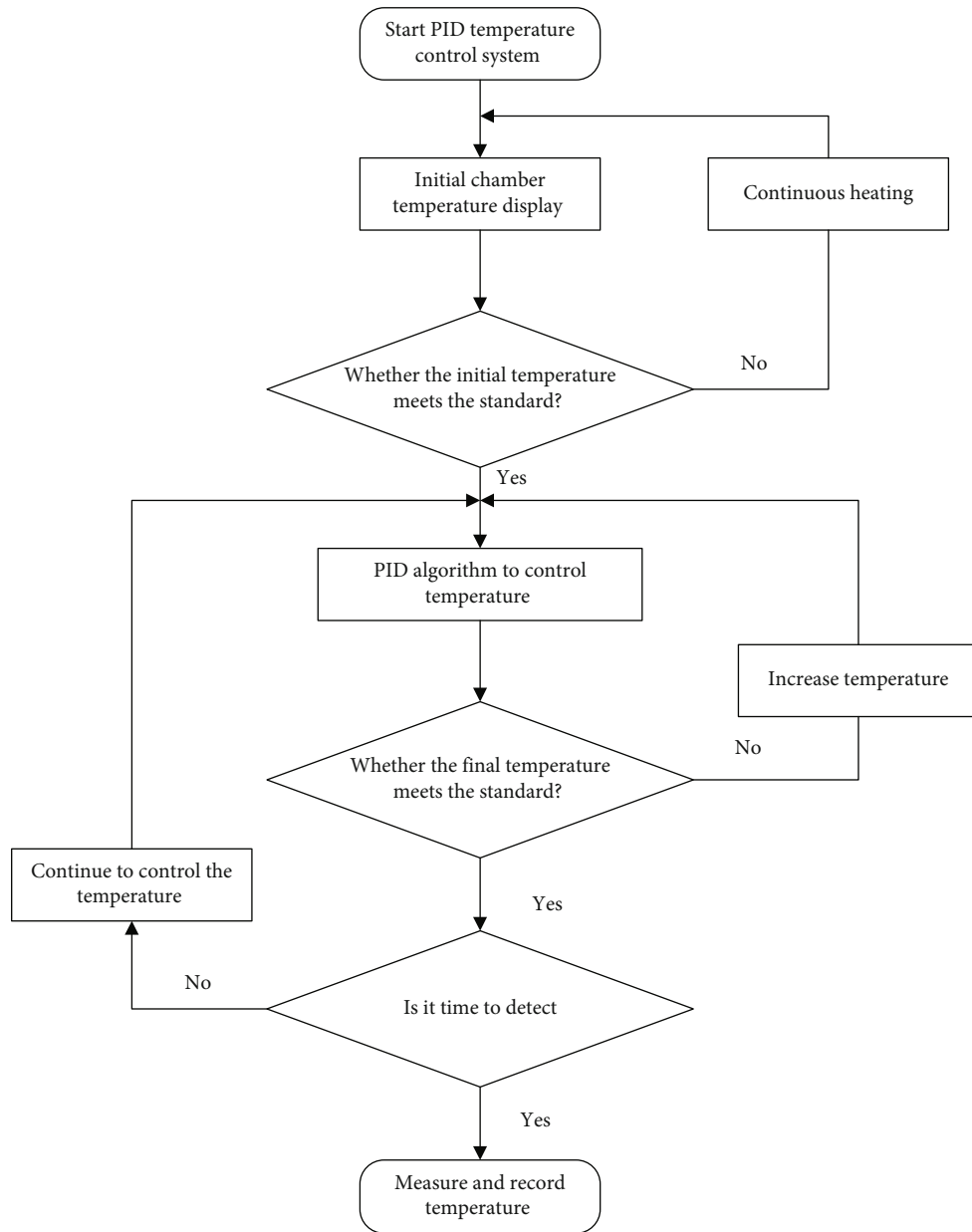


FIGURE 6: Basic flow of temperature control using the PID temperature control algorithm.

where  $t$  represents the quantization factor of the fuzzy value. The amount of fuzzy control can also be calculated [30]. The calculation equation is as follows:

$$V = (R \times RB) \bullet T, \quad (25)$$

where  $V$  represents the amount of control fuzzy,  $R$  represents the fuzzy number of input values,  $T$  is the fuzzy coefficient,  $\times$  represents the direct operation of fuzzy values, and  $\bullet$  the synthesis operation of fuzzy values [31]. The discrete domain calculation equation of the fuzzy value is

$$v_o = \frac{\sum_{i=1}^n v_i \mu(v_i)}{\sum_{i=1}^n \mu(v_i)}, \quad (26)$$

where  $v_o$  is the accuracy of the output value and  $v_i$  represents the variable of the output value. In addition, the calculation equations of three control parameters  $P$ ,  $I$ , and  $D$  are [32]

$$K_P = K_{P0} + \{Ei, ECi\}_P, \quad (27)$$

$$K_I = K_{I0} + \{Ei, ECi\}_I, \quad (28)$$

$$K_D = K_{D0} + \{Ei + ECi\}_D, \quad (29)$$

where  $K_{P0}$ ,  $K_{I0}$ , and  $K_{D0}$  represent the initial values of the three control parameters  $P$ ,  $I$ , and  $D$ , respectively. Through the adjustment of the PID temperature control algorithm, the results of the final three parameters can be calculated as  $K_P$ ,  $K_I$ , and  $K_D$  [33].

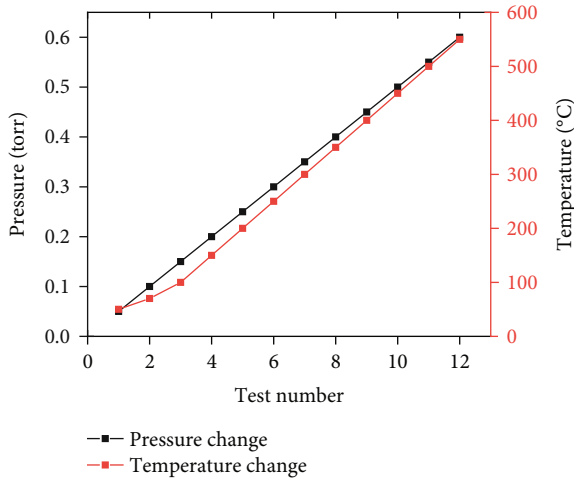


FIGURE 7: Relevant variables.

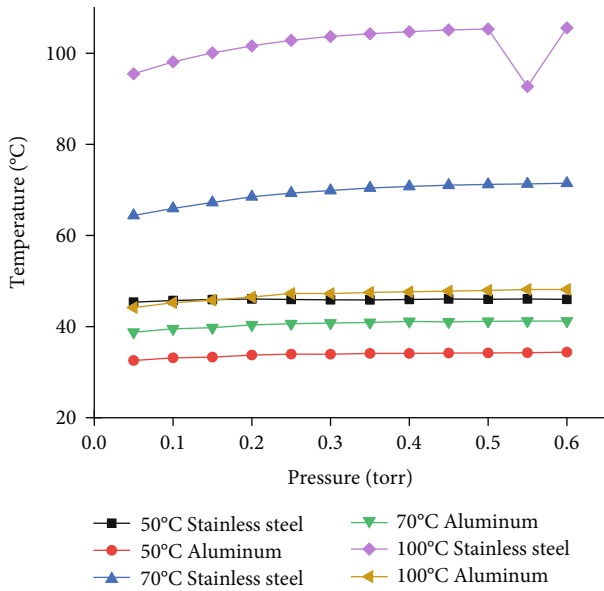


FIGURE 8: Record results of the PID temperature control algorithm at 50°C, 70°C, and 100°C.

2.4. Modeling of PID Based on ALD Reaction Chamber. The PID temperature control algorithm based on the ALD reaction chamber is studied, and the specific equipment used is the dual cavity ALD system. Figure 5 shows the basic structural framework of the dual cavity ALD system.

Figure 5 shows that the PID temperature control algorithm can be compared with different materials with strong responses in the dual cavity ALD system. After that, the PID temperature control algorithm can automatically select ALD chamber materials and improve its performance through the feedback of different materials [34]. The PID temperature control algorithm is studied by recording and analyzing the reaction chamber temperature in the ALD process system [35]. Figure 6 shows the basic process of using the PID temperature control system to control the reaction chamber temperature in the ALD process system.

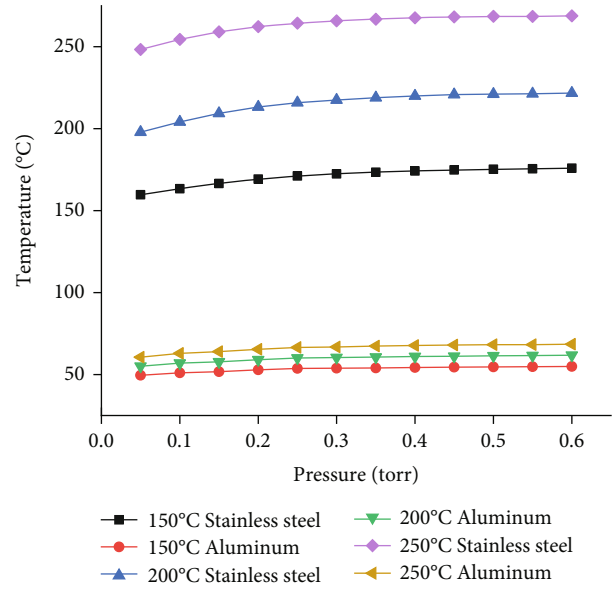


FIGURE 9: Record results of the PID temperature control algorithm at 150°C, 200°C, and 250°C.

Figure 6 shows that at the beginning, the reaction chamber of the ALD process needs to be heated, and the temperature should reach the initial temperature required by the experiment. Then, the initial temperature of the chamber is detected to judge whether the temperature meets the standard. If the temperature does not meet the standard, the reaction chamber needs to be heated again. If the temperature meets the standard, the next step is continued. The PID temperature control algorithm is used to control the temperature in the reaction chamber. During the control process, it is necessary to change the chamber temperature regularly and then detect whether the temperature meets the standard. If it does not meet the standard, it needs to be reheated. If it meets the standard, go to the next step to judge whether it is time to record. If the temperature cannot be recorded, continue maintaining the temperature by PID. If it is recorded, the temperature is recorded and adjusted in real time, and the research results are analyzed according to the recorded data.

### 3. Research Results

3.1. ALD Reaction Chamber. According to the above research methods, the PID temperature control algorithm is studied based on different materials of the ALD reaction chamber. Figure 7 shows the research conditions of other chamber materials.

Figure 7 shows that the chambers of the two materials are experimentally studied under the same conditions, in which the pressure changes are 0.05, 0.1, 0.15, 0.2, 0.25, 0.3, 0.35, 0.4, 0.45, 0.5, 0.55, and 0.6, respectively, and the temperature changes are 50, 70, 100, 150, 200, 250, 300, 350, 400, 450, 500, and 550°C, respectively. The research under different pressures and temperatures can reflect the temperature tolerance of the two materials and test the



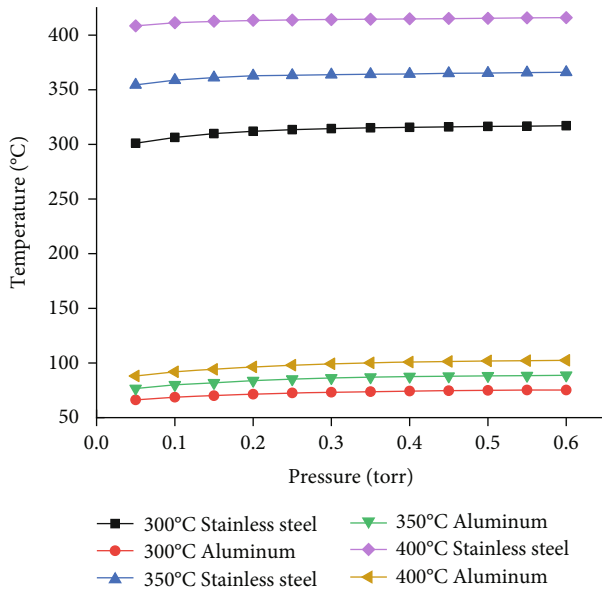


FIGURE 10: Record results of the PID temperature control algorithm at 300°C, 350°C, and 400°C.

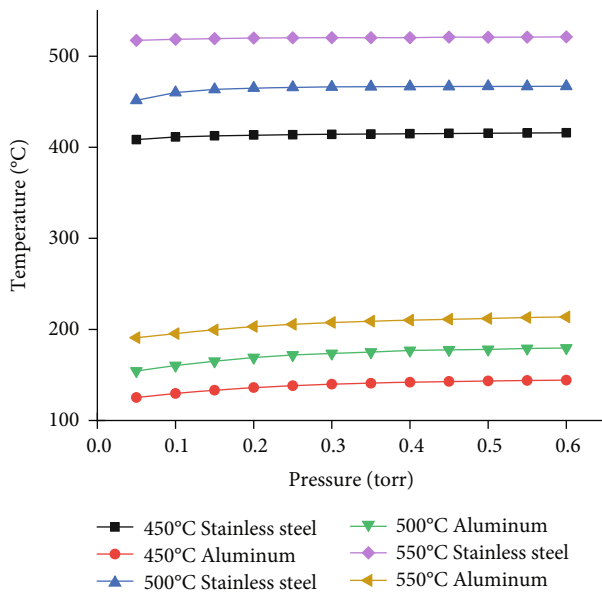


FIGURE 11: Record results of the PID temperature control algorithm at 450°C, 500°C, and 550°C.

influence of the two materials on the temperature tolerance under different pressure conditions

**3.2. PID Research and Analysis Based on ALD.** Through the research on the PID temperature control test for reaction chambers of different materials under different conditions, the heat resistance and pressure resistance of other materials are analyzed, which can reveal the service status of the PID temperature control algorithm. This verifies the performance of the PID temperature control algorithm through different materials and improves the authenticity and feasi-

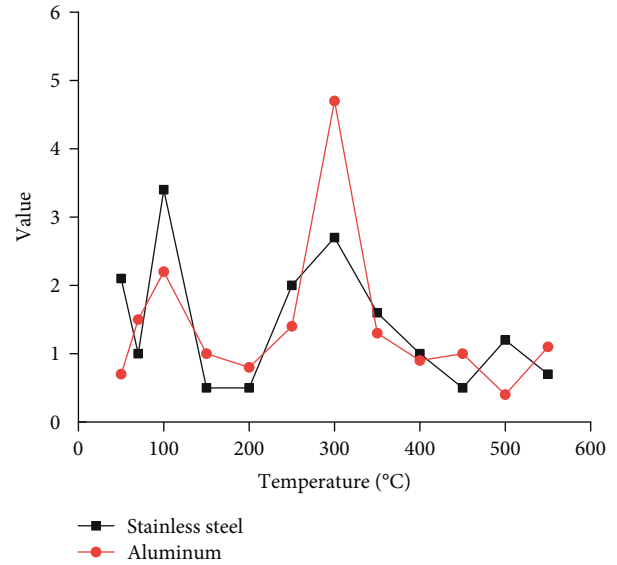


FIGURE 12: Comparison of the errors of temperature control systems.

bility of the research. Figure 8 shows the temperature recording results.

Figure 8 shows that when the results of the PID temperature control records are 50°C, 70°C, and 100°C, the temperature of the stainless steel chamber is at 100°C with an error of about  $\pm 5^\circ\text{C}$ . The temperature of the aluminum chamber is at 50°C, which is maintained at about 30°C, and the error is about  $\pm 3^\circ\text{C}$ .

Figure 9 shows that when the results of the PID temperature control algorithm are 150°C, 200°C, and 250°C, the temperature of the stainless steel chamber is at 250°C with an error of about  $\pm 2^\circ\text{C}$ . The temperature of the aluminum chamber is at 150°C with an error of about  $\pm 1^\circ\text{C}$ .

Figure 10 shows that when the results of the PID temperature control algorithm are 300°C, 350°C, and 400°C, the temperature of the stainless steel chamber is at 400°C with an error of about  $\pm 1^\circ\text{C}$ . The temperature of the aluminum chamber is at 300°C with an error of about  $\pm 3^\circ\text{C}$ .

Figure 11 shows that when the results of the PID temperature control algorithm are 450°C, 500°C, and 550°C, the temperature of the stainless steel chamber is at 550°C with an error of about  $\pm 3^\circ\text{C}$ . The temperature of the aluminum chamber is at 450°C with an error of about  $\pm 5^\circ\text{C}$ . Figure 12 shows the difference between the predicted error and the actual error of the two materials.

Figure 12 shows that the maximum difference between the prediction error of the cavity temperature of stainless steel and its actual error is about  $3^\circ\text{C}$ . In contrast, the maximum difference between the prediction error of the cavity temperature of aluminum and the actual error is about  $5^\circ\text{C}$ . Therefore, the PID temperature control system is reasonable for error control.

Figures 8–11 show that the temperature changes of the two materials are not significant by applying the PID temperature control algorithm to the reaction chambers of the two materials under different conditions. It is concluded that

the pressure has little effect on the temperature resistance of the ALD reaction chamber. Still, the temperature of the reaction chamber varies significantly at different initial temperatures. When the initial temperature is 50°C, the temperature difference between the two materials is not significant, maintaining at about 20°C. Therefore, the reaction chambers of these two materials are suitable for temperature regulation with a temperature control system above 50°C. With the initial temperature increase, the temperature difference between different materials begins to increase gradually under the PID temperature control algorithm. The temperature difference has risen to about 50°C under the condition of 70°C. At 550°C, the reaction chamber gap of the two materials reached the maximum, maintaining at about 320°C. However, when the change of the reaction chamber of the two materials under the PID temperature control algorithm is analyzed, it is found that the temperature change of stainless steel is more significant than that of the aluminum chamber. The temperature tolerance of the reaction chamber made of stainless steel is sensitive. When the heating temperature increases, the temperature of the stainless steel reaction chamber increases rapidly, while the temperature of the aluminum reaction chamber decreases. This proves that the temperature tolerance of the aluminum reaction chamber is high. Still, the overall temperature of the reaction chamber made of different materials does not change much under the PID temperature control algorithm, and the performance of the PID temperature control system is also stable under different pressures. The curve remains stable and in an ideal state. This shows that the PID temperature control algorithm can be used under different temperatures and pressures.

#### 4. Conclusion

The PID temperature control algorithm is used to analyze its application to the ALD reaction chamber. The test is taken in the reaction chamber with different materials, different reaction temperatures, and different pressure changes. The simulation experiment found that the reaction chambers with different materials have different tolerance sensitivity to different temperature changes. Among them, the temperature sensitivity of stainless steel is more significant than aluminum, and the difference between the two is very large. Then, the temperature changes of the two materials under different pressure conditions are compared. The results show that the pressure changes have little effect on the temperature changes of the reaction chamber of different materials. Finally, it is concluded that different temperature changes and different pressure changes have little influence on the PID temperature control algorithm. This proves that the PID temperature control algorithm can be used normally in reaction chambers with different materials, temperatures, and pressures. The optimization of the traditional PID algorithm found that the error of the optimization algorithm is fewer in the temperature control process, and the maximum difference between the prediction error and the actual error is 3°C and 5°C. The optimization results of the PID temperature control algorithm are ideal. Although this study pro-

vides a lot of research data, the sample size used in the comparison is still small. The size will be expanded in the future, and the practical application of the PID temperature control algorithm will be strengthened.

#### Data Availability

The labeled dataset used to support the findings of this study are available from the corresponding author upon request.

#### Conflicts of Interest

The author declares no competing interests.

#### References

- [1] H. B. Zhang, S. Christopher, and L. Marshall, "ALD: new catalyst synthesis and modification process (English)," *Chinese Journal of Catalysis*, vol. 40, no. 9, pp. 91–103, 2019.
- [2] R. Li, F. Wu, P. Hou, and H. Zou, "Performance assessment of FO-PID temperature control system using a fractional order LQG benchmark [J]," *IEEE Access*, vol. 8, no. 99, pp. 116653–116662, 2020.
- [3] N. Gilbert and F. V. Leeuwen, "Chromatin modified in a molecular reaction chamber," *Nature*, vol. 579, no. 7800, pp. 503–504, 2020.
- [4] S. Tomer, A. Vandana, J. Panigrahi, R. Srivastava, and C. M. S. Rauthan, "Importance of precursor delivery mechanism for Tetra-kis-ethylmethylaminohafnium/water atomic layer deposition process," *Thin Solid Films*, vol. 692, p. 137629, 2019.
- [5] H. Huang, S. Zhang, Z. Yang et al., "Modified Smith fuzzy PID temperature control in an oil-replenishing device for deep-sea hydraulic system," *Ocean Engineering*, vol. 149, no. 1, pp. 14–22, 2018.
- [6] M. Li, W. Wu, and X. Yang, "Research on fuzzy fractional order PID control of liquid temperature in displacement digester [J]," *Palpu Chongi Gisul/Journal of Korea Technical Association of the Pulp and Paper Industry*, vol. 52, no. 5, pp. 15–30, 2020.
- [7] F. Grillo, V. B. Hao, D. L. Zara, and A. A. I. Aranink, "From single atoms to nanoparticles: autocatalysis and metal aggregation in atomic layer deposition of Pt on TiO<sub>2</sub> nanopowder," *Small*, vol. 14, no. 23, pp. 45–46, 2018.
- [8] Y. Mu, T. L. Hu, C. Chen, H. Gong, and S. J. Li, "Development of temperature control system of DFB laser using analog PID control [J]," *Infrared and Laser Engineering*, vol. 48, no. 4, p. 405001, 2019.
- [9] D. M. Fryauf, A. C. Phillips, M. J. Bolte, A. Feldman, G. S. Tompa, and N. P. Kobayashi, "Scaling atomic layer deposition to astronomical optic sizes: low-temperature aluminum oxide in a meter-sized chamber [J]," *ACS Applied Materials & Interfaces*, vol. 10, no. 48, pp. 41678–41689, 2018.
- [10] E. R. Borujeny, O. Sendetskyi, and M. D. Fleischaer, "Low thermal budget heteroepitaxial gallium oxide thin films enabled by atomic layer deposition [J]," *ACS Applied Materials and Interfaces*, vol. 12, no. 39, pp. 44225–44237, 2020.
- [11] Y. Wu, M. H. Raza, Y. C. Chen, P. Amsalem, and N. Pinna, "A self-limited atomic layer deposition of WS<sub>2</sub> based on the chemisorption and reduction of Bis(t-

- butylimino)bis(dimethylamino) complexes [J],” *Chemistry of Materials*, vol. 31, no. 6, pp. 1881–1890, 2019.
- [12] A. Alnuaimi, I. Almansouri, I. Saadat, and A. Nayfeh, “High performance graphene-silicon Schottky junction solar cells with  $\text{HfO}_2$  interfacial layer grown by atomic layer deposition,” *Solar Energy*, vol. 164, pp. 174–179, 2018.
- [13] M. Snure, S. R. Vangala, T. Prusnick, G. Grzybowski, and K. D. Leedy, “Two-dimensional BN buffer for plasma enhanced atomic layer deposition of  $\text{Al}_2\text{O}_3$  gate dielectrics on graphene field effect transistors,” *Scientific Reports*, vol. 10, no. 1, p. 14699, 2020.
- [14] Z. Zhu, S. Merdes, and O. Ylivaara, “ $\text{Al}_2\text{O}_3$  thin films prepared by a combined thermal-plasma atomic layer deposition process at low temperature for encapsulation applications,” *Physica Status Solidi (a)*, vol. 217, no. 8, 2020.
- [15] J. Q. Li, J. P. Li, J. Z. Wang, and J. M. Sun, “Structure and dielectric property of high-k  $\text{ZrO}_2$  films grown by atomic layer deposition using tetrakis(dimethylamido)zirconium and ozone,” *Nanoscale Research Letters*, vol. 14, no. 1, p. 154, 2020.
- [16] S. Kui, W. Ming, Y. Guo, and X. Feng, “Improving the performance of thermoelectric materials by atomic layer deposition-based grain boundary engineering,” *Structural Chemistry*, vol. 39, no. 5, p. 7, 2020.
- [17] J. Zhang, H. Sun, Y. Qi, and S. Deng, “Temperature control strategy of incubator based on RBF neural network PID,” *World Scientific Research Journal*, vol. 6, no. 1, pp. 7–15, 2020.
- [18] Z. A. Zhe, K. A. Ye, and L. A. Chang, “Atomic layer deposition-induced integration of N-doped carbon particles on carbon foam for flexible supercapacitor,” *Journal of Inorganic Materials (English)*, vol. 6, no. 1, pp. 209–215, 2020.
- [19] D. Gaboriau, M. Boniface, A. Valero et al., “Atomic layer deposition alumina-passivated silicon nanowires: probing the transition from electrochemical double-layer capacitor to electrolytic capacitor[J],” *ACS Applied Materials & Interfaces*, vol. 9, no. 15, p. 13761, 2017.
- [20] S. Zhang, E. Yu, S. Gates et al., “Helium interactions with alumina formed by atomic layer deposition show potential for mitigating problems with excess helium in spent nuclear fuel,” *Journal of Nuclear Materials*, vol. 499, pp. 301–311, 2018.
- [21] Y. Yang, L. Na, and J. Sun, “Intense electroluminescence from  $\text{Al}_2\text{O}_3/\text{Tb}_2\text{O}_3$  nanolaminate films fabricated by atomic layer deposition on silicon,” *Optics Express*, vol. 26, no. 7, pp. 9344–9352, 2018.
- [22] X. Shen, C. Li, C. Shi et al., “Core-shell structured ceramic non-woven separators by atomic layer deposition for safe lithium-ion batteries,” *Applied Surface Science*, vol. 441, no. 31, pp. 165–173, 2018.
- [23] Z. Ou, Y. Yang, and J. Sun, “Electroluminescent  $\text{Yb}_2\text{O}_3:\text{Er}$  and  $\text{Yb}_2\text{Si}_2\text{O}_7:\text{Er}$  nanolaminate films fabricated by atomic layer deposition on silicon,” *Optical Materials*, vol. 80, pp. 209–215, 2018.
- [24] X. U. Zhi, X. U. Ming, W. Cheng, H. Peng, and Y. Ding, “High-precision, temperature control based on grading-structure and PID-feedback strategies,” *Transactions of the Japan Society for Aeronautical and Space Sciences*, vol. 61, no. 2, pp. 51–59, 2018.
- [25] M. M. Gani, M. S. Islam, and M. A. Ullah, “Optimal PID tuning for controlling the temperature of electric furnace by genetic algorithm [J],” *SN Applied ences*, vol. 1, no. 8, p. 880, 2019.
- [26] A. Magalhes, J. D. Backer, and G. Bolmsj, “Thermal dissipation effect on temperature-controlled friction stir welding [J],” *Soldagem & Inspeção*, vol. 24, no. 3, pp. 24–32, 2019.
- [27] H. W. Yin, Y. J. Zhao, and X. G. Nie, “Design of temperature control and bipolar PID control algorithm for heating room based on ARM,” *Journal of Pingdingshan University*, vol. 34, pp. 35–40, 2019.
- [28] J. Możaryn, J. Petryszyn, and S. Ozana, “PLC based fractional-order PID temperature control in pipeline: design procedure and experimental evaluation [J],” *Meccanica*, vol. 56, no. 4, pp. 855–871, 2021.
- [29] Y. Cheng, “Research on intelligent control of an agricultural greenhouse based on fuzzy PID control [J],” *Journal of Environmental Engineering and Science*, vol. 15, no. 3, pp. 113–118, 2020.
- [30] M. F. Al Andzar and R. D. Puriyanto, “PID control for temperature and motor speed based on PLC [J],” *Signal and Image Processing Letters*, vol. 1, no. 1, pp. 7–13, 2019.
- [31] A. Shikano, L. Tonthat, and S. Yabukami, “A simple and high-accuracy PID-based temperature control system for magnetic hyperthermia using fiber optic thermometer,” *IEEE Transactions on Electrical and Electronic Engineering*, vol. 16, no. 5, pp. 807–809, 2021.
- [32] S. J. Hammoodi, K. S. Flayyih, and A. R. Hamad, “Design and implementation speed control system of DC motor based on PID control and matlab simulink [J],” *International Journal of Power Electronics and Drive Systems*, vol. 11, no. 1, p. 127, 2020.
- [33] Q. Cheng and K. Zhang, “Design of temperature intelligent PID control system based on genetic algorithm,” *Journal of Shenyang University of Technology*, vol. 40, no. 4, pp. 459–463, 2018.
- [34] L. Hua, C. T. Zhang, W. Q. Lu, and J. Wang, “Stove temperature control application simulation based on fuzzy self-adaptive PID,” *Journal of Guangxi University of Technology*, vol. 29, pp. 37–42, 2018.
- [35] H. Liang, Z. K. Sang, Y. Z. Wu, Y. H. Zhang, and R. Zhao, “High precision temperature control performance of a PID neural network- controlled heater under complex outdoor conditions,” *Applied Thermal Engineering*, vol. 195, no. 1, p. 117234, 2021.